

Molecular simulation of phase equilibria for mixtures of polar and non-polar components

J. J. Potoff, J. R. Errington and A. Z. Panagiotopoulos *

Institute for Physical Science and Technology
and Department of Chemical Engineering,
University of Maryland, College Park, MD 20742-2431

June 10, 1999

Submitted to *Molecular Physics*

*To whom correspondence should be addressed. E-mail: thanos@ipst.umd.edu

Abstract

Grand canonical histogram-reweighting Monte Carlo simulations were used to obtain the phase behavior of several binary mixtures. The main goal of this work was to test the predictive capabilities of recently developed intermolecular potential models that accurately reproduce the phase behavior of pure components. These united-atom potentials utilize the exponential-6 functional form for repulsive and dispersion interactions and fixed point charges for electrostatic interactions. The mixtures studied were *n*-pentane/methane, ethane/CO₂, propane/CO₂, *n*-pentane/CO₂, H₂O/ethane, CH₃OH/*n*-hexane and CH₃OH/CO₂. The conventional Lorentz-Berthelot combining rules, as well as a set of combining rules due to Kong [*J. Chem. Phys.* **59**, 2464 (1973)] were used to obtain unlike-pair potential parameters. The Lorentz-Berthelot rules generally result in more attractive unlike-pair interactions than the Kong rules. For the *n*-alkane/CO₂ systems, predicted phase diagrams are in excellent agreement with experiment when the Kong combining rules are used. For mixtures with CH₃OH and H₂O, the Lorentz-Berthelot rules yield better agreement with experiment than the Kong rules, but statistically significant differences remain. Our results suggest that relatively simple intermolecular potential models can be used to predict the phase behavior of broad classes of binary systems. For mixtures with large differences in polar

character of the components, however, present models do not predict the phase behavior in quantitative agreement with experiment. New models that include higher order interactions such as polarizability may be suitable for this purpose, a hypothesis that will need to be tested in the future.

1 Introduction

Molecular simulation methods for prediction of phase equilibria from a detailed atomistic description of a system have evolved rapidly in recent years. Algorithms such as Gibbs ensemble Monte Carlo [1–3] have greatly simplified the determination of phase coexistence properties for a fluid with given intermolecular interactions. Configurational-bias sampling [4–6], thermodynamic scaling Monte Carlo [7–12] and expanded ensemble methods [13] have significantly broadened the range of systems for which the phase behavior can be studied by simulation.

Grand canonical Monte Carlo simulations combined with histogram-reweighting methods [14–18], provide a powerful method for phase equilibrium calculations. By storing data on the frequency of energy and particle numbers in the form of a histogram, it is possible to determine the free energy of a system over a range of thermodynamic conditions from a limited number of simulations. A limitation of the Gibbs ensemble method is that finite-size effects near the critical point are often difficult to characterize and control, due to the variable extent of the two simulation regions [3, 19–22]. By contrast, for grand canonical Monte Carlo simulations, such effects are well understood and easily controlled [18, 23]. In addition, grand canonical Monte Carlo simulations appear to have an increased statistical efficiency when compared to Gibbs ensemble Monte Carlo [18] for identical systems and conditions.

Molecular simulation methods can now be used to predict the phase co-

existence properties of complex, industrially relevant fluids. The main limitation in the prediction of pure component and mixture phase behavior is the lack of accurate intermolecular potentials. Recent studies have shown that united-atom models can achieve near experimental accuracy in phase equilibrium calculations for pure fluids. Parameters are available for several fluids including *n*-alkanes [24–26], CO₂ [27, 28], CH₃OH [28] and H₂O [29]. While the models accurately reproduce the pure fluid phase behavior, they have only been tested for a limited number of primarily non-polar mixtures [26, 30–34]. Significant deviations from experiment have been found in the predicted phase behavior for certain long-chain *n*-alkane [30], asymmetric *n*-alkane [32] and *n*-alkane/H₂O [33] mixtures. This raises questions about the predictive power of these models.

In this work, grand canonical histogram-reweighting Monte Carlo simulations are used to study a series of binary mixtures with polar and non-polar components. These mixtures are *n*-pentane/methane, ethane/CO₂, propane/CO₂, *n*-pentane/CO₂, H₂O/ethane, CH₃OH/*n*-hexane, and CH₃OH/CO₂. The exponential-6 functional form was used for repulsive and dispersive interactions. Fixed point charges were used for electrostatic interactions. Pure component potential parameters have been determined for these components from Hamiltonian-scaling grand canonical Monte Carlo simulations [17, 26, 28]. A comparison is made between mixture phase diagrams predicted by the Lorentz-Berthelot [35] and Kong [36] combining rules for unlike-pair interactions. The Lorentz-Berthelot rules have been used exten-

sively to obtain unlike-pair parameters in previous simulation work, but their theoretical justification is weak. The Kong combining rules generally result in less attractive unlike-pair interactions and were originally proposed to obtain better agreement with experiment for noble-gas mixtures.

The plan of this paper is as follows. In the next section, a discussion of the histogram-reweighting technique applied to a grand canonical Monte Carlo simulation for a multi-component system is presented. In section 3, the details of the united atom models used in this study are given. Computational details are given in section 4. Section 5 contains the results of our simulation study for a series of binary mixtures. A comparison is made between results using Lorentz-Berthelot and Kong combining rules and experimental data. Conclusions are given in section 6.

2 Simulation Methodology

Histogram techniques can be used to provide accurate data for the free energy of a system over a range of thermodynamic conditions [14,15]. In this section we give a brief overview of histogram-reweighting as it applies to a simulation for n components in the grand canonical ensemble.

In the grand canonical ensemble, the number of particles N_1, \dots, N_n and energy E fluctuate while the temperature T , volume V and chemical potentials μ_1, \dots, μ_n are input parameters of the simulation. Over the course of the simulation, a histogram containing the number of particles of each species

and the energy is collected. The probability of observing a configuration with a given number of particles and configurational energy is:

$$P(N_1, \dots, N_n, E) = \frac{\Omega(N_1, \dots, N_n, V, E) \exp(-\beta E + \sum_{i=1}^n \beta \mu_i N_i)}{\Xi(\mu_1, \dots, \mu_n, V, E)}, \quad (1)$$

where Ω is the microcanonical density of states and Ξ is the grand canonical partition function. For pure fluids, it is convenient to store data in the form of a two dimensional histogram. For multi-component systems, however, the range of phase space covered by a simulation can be quite large. Instead, it is more efficient to record periodically the set of N_1, \dots, N_n, E values. The required probability distribution is extracted from this list at the end of the simulation.

In general, it is not possible to cover all thermodynamic states of interest from a single simulation. Multiple simulations are required at various chemical potentials and temperatures. This is illustrated schematically in Figure 1. The two runs for which one-dimensional histograms of $P(N)$ versus N are being collected each covers a different region of densities. The histograms which result from the simulations are combined according to the method outlined by Ferrenberg and Swendsen [15, 16] to form a unified distribution which can be reweighted to the conditions of interest. In order to combine multiple histograms, a reasonable amount of overlap must be present between neighboring histograms. Again, a schematic illustration of this process for the case of the data of Figure 1 is given in Figure 2. The transformation $\ln[P(N)] - \beta \mu N$, according to equation 1 applied to a one-component system

at constant temperature, should result in a quantity equal to $\ln Q(N, V, T)$ within an additive constant. The method of Ferrenberg and Swendsen provides a value of the constant so that an optimum overall free energy curve is obtained over the range of densities covered by the multiple histograms.

When determining phase coexistence properties, there must be a free energy link between the liquid and vapor at the conditions of interest. In most cases it is convenient to bridge the liquid and vapor regions with a run near the critical point. Additional histograms are added on the liquid and vapor sides of the coexistence curve. This avoids the problem of the formation of interfaces and the need to cross over the free energy barrier which grows as one moves away from the critical point. An alternative method is to overcome the large free energy barrier separating liquid from vapor at low temperatures through the application of the multicanonical method of Berg and Neuhaus [37].

The pressure of the system is related to the area under the probability distribution by:

$$\beta p = \frac{\ln \Xi(\mu_1, \dots, \mu_n, V, E)}{V} + \text{constant} = \ln \sum_{N_1, \dots, N_n, E} \Omega(N_1, \dots, N_n, V, E) \exp(-\beta E + \sum_{i=1}^n \beta \mu_i N_i). \quad (2)$$

To determine the additive constant in equation 2, the partition function is calculated at low densities. A plot of $\ln \Xi$ vs. N gives a straight line of unit slope, which shows the system behaves as an idea gas at these conditions. It is possible to extrapolate $\ln \Xi$ to the $N = 0$ limit, with the y intercept

representing the additive constant.

Near phase coexistence a bimodal distribution of densities is expected. Phase coexistence is determined by adjusting the chemical potentials of the two components until equal area is found under the two peaks. Coexistence densities and mole fractions are calculated by taking the weighted average under each peak.

Once a sufficient number of histograms have been collected and combined so that the region of temperatures, densities and compositions of interest have been covered, results for any property of interest can be obtained at any state point within the covered region. Our results shown in Figures 3 to 9 are represented by continuous curves for this reason. The slight "wiggles" present in the curves are a reflection of imperfect sampling of the underlying histograms, expected for any simulation of finite length.

3 Potential Models

The *n*-alkane, CO₂, H₂O and CH₃OH models used in this work are based on a united-atom representation. Hydrogens are added explicitly only to the hydroxyl groups of H₂O and CH₃OH as partial charges. These hydrogens interact only through coulombic forces. Non-bonded interactions between groups that are separated by more than three groups or belong to different molecules are given by a pairwise additive exponential-6 potential,

$$U^{exp-6}(r_{ij}) = \begin{cases} \frac{\varepsilon}{1 - 6/\alpha} \left[\frac{6}{\alpha} \exp\left(\alpha \left[1 - \frac{r}{r_m}\right]\right) - \left(\frac{r_m}{r}\right)^6 \right] & r_{ij} > r_{max} \\ \infty & r_{ij} < r_{max}, \end{cases} \quad (3)$$

where ε , r_m and α are model parameters. The radial distance at which the potential is a minimum is given by r_m . The cutoff distance r_{max} is the smallest positive value for which $du(r)/dr = 0$ and is obtained from the iterative solution of equation 3. At very short distances the exponential-6 potential becomes negative, which necessitates the use of a cutoff distance in grand canonical Monte Carlo simulations.

The following groups were used as building blocks: CH₃, CH₂, C and O (in CO₂), OH (in H₂O) and OH (in CH₃OH). The exponential-6 and charge parameters were obtained from experimental saturated liquid and vapor densities, vapor pressures and critical points [26,28]. These parameters are listed in Table 1. The size parameter σ listed in the table is the distance for which the potential is zero and is obtained numerically from Equation 3.

Groups are separated by fixed bond lengths, which are listed in Table 2. Bond bending is given by a harmonic potential,

$$U(\theta) = k_\theta(\theta - \theta_{eq})^2/2, \quad (4)$$

where the force constant $k_\theta/k_b = 62500$ K/rad² [38] (k_b is Boltzmann's constant) and the equilibrium angle θ_{eq} is set to 114.0° for the n -alkanes. For the hydrogen in the methanol OH group $k_\theta/k_b = 55000$ K/rad² and $\theta_{eq} = 108.5^\circ$ [39]. The H₂O and CO₂ models used in this work have fixed

bond angles and do not use a bond bending potential. In H₂O, the H-O-H bond angle is set at 109.5°. For CO₂, the O-C-O bond angle is fixed at 180°. The bond torsion angles ϕ for the n -alkanes are governed by the OPLS united-atom torsional potential [40],

$$U(\phi) = U_o + \frac{c_1}{2}[1 + \cos(\phi)] + \frac{c_2}{2}[1 - \cos(2\phi)] + \frac{c_3}{2}[1 + \cos(3\phi)]. \quad (5)$$

Model parameters were taken from Smit *et al.* [41], with $U_o = 0$ K, $c_1/k_b = 355.03$ K, $c_2/k_b = -68.19$ K and $c_3/k_b = 791.32$ K.

For molecules such as H₂O, CO₂ and CH₃OH, which have electrostatic interactions, the potential may be written as:

$$U(r_{ij}) = U^{exp-6} + \frac{q_i q_j}{4\pi\epsilon_0 r_{ij}}, \quad (6)$$

where q_i refers to the partial charge on each site and ϵ_0 is the permittivity of a vacuum. The partial charges carried by each group are listed in Table 1.

Two sets of combining rules were used for interactions between groups belonging to unlike molecules. For interactions between groups of like molecules, pure component parameters had been determined using the Lorentz-Bethelot combining rules, so these parameters were used without changes. For all systems we ran simulations with the Lorentz-Berthelot combining rules,

$$\sigma_{ij} = (\sigma_{ii} + \sigma_{jj})/2, \quad (7)$$

$$\epsilon_{ij} = \sqrt{\epsilon_{ii}\epsilon_{jj}}, \quad (8)$$

For the exponent in the repulsive part of the potential the following com-

binning rule [42] was used together with the Lorentz-Berthelot rules:

$$\alpha_{ij} = \sqrt{\alpha_{ii}\alpha_{jj}}. \quad (9)$$

In general, the geometric mean combining rule has been found to overestimate the unlike-pair interactions for rare gases [35]. A number of other combining rules for unlike-pair potentials have been proposed by Fender and Halsey [43], Smith [44] and Kong [36]. The most successful of these are based on “atomic distortion” models, where the interaction of two atoms is assumed to cause a distortion in the electron clouds surrounding each atom.

According to Smith [44], the repulsive potential between two atoms is simply the sum of the distortion energies internal to atom A and B, which may be written as:

$$U_{AB}^{rep}(R) = \frac{1}{2}[U_{AA}^{rep}(2r_A) + U_{BB}^{rep}(2r_B)], \quad (10)$$

where r_A is the radial distance of the distortion plane away from atom A, r_B is the radial distance of the distortion plane away from atom B and $R = r_A + r_B$.

The location of the distortion plane is subject to the following constraint:

$$\left. \frac{dU_{AA}^{rep}(R)}{dR} \right|_{R=2r_A} = \left. \frac{dU_{BB}^{rep}(R)}{dR} \right|_{R=2r_B}, \quad (11)$$

that stipulates that the total energy must be minimized, resulting in equal and opposite restoring forces in each atom.

Kong extended the work of Smith by combining the “atomic distortion” model for the repulsive interactions with the familiar geometric mean rule for the attractive interactions [36]. The Kong combining rules have been shown

to yield more accurate results for the unlike-pair interactions between non-polar molecules that have large differences in size and/or potential strength. From 10 and 11, the Kong combining rules for the exponential-6 potential were obtained:

$$\left[\frac{\varepsilon_{12}\alpha_{12} \exp(\alpha_{12})}{(\alpha_{12} - 6)\sigma_{12}} \right]^{\frac{2\sigma_{12}}{\alpha_{12}}} = \left[\frac{\varepsilon_{11}\alpha_{11} \exp(\alpha_{11})}{(\alpha_{11} - 6)\sigma_{11}} \right]^{\frac{\sigma_{11}}{\alpha_{11}}} \left[\frac{\varepsilon_{22}\alpha_{22} \exp(\alpha_{22})}{(\alpha_{22} - 6)\sigma_{22}} \right]^{\frac{2\sigma_{22}}{\alpha_{22}}}, \quad (12)$$

$$\left[\frac{\varepsilon_{12}\alpha_{12}\sigma_{12}^6}{(\alpha_{12} - 6)} \right] = \left[\frac{\varepsilon_{11}\alpha_{11}\sigma_{11}^6}{(\alpha_{11} - 6)} \times \frac{\varepsilon_{22}\alpha_{22}\sigma_{22}^6}{(\alpha_{22} - 6)} \right]^{\frac{1}{2}}, \quad (13)$$

$$\frac{\sigma_{12}}{\alpha_{12}} = \frac{1}{2} \left[\frac{\sigma_{11}}{\alpha_{11}} + \frac{\sigma_{22}}{\alpha_{22}} \right]. \quad (14)$$

Solution of the above equations for the cross parameters is accomplished through an iterative process. A comparison of the unlike-pair parameters calculated via the Lorentz-Berthelot and Kong combining rules is given in Table 3. Values are listed as departures from the Lorentz-Berthelot combining rules, $1 - X_{Kong}/X_{L-B}$, where $X = \varepsilon_{ij}$, σ_{ij} or α_{ij} depending on the quantity of interest. Deviations of the parameters resulting from the Kong combining rules from those from the Lorentz-Berthelot for ε_{ij} are positive in all cases, except for O(CO₂)-O(CH₃OH). Deviations increase with increasing asymmetry between potential parameters. Deviation for σ_{ij} are negative and approximately an order of magnitude lower than deviations for ε_{ij} . The α_{ij} parameter also exhibits small negative deviations.

4 Computational Details

Grand canonical histogram-reweighting Monte Carlo simulations were employed for all our calculations. Monte Carlo moves consisted of 15% particle displacements, 15% rotations, 35% insertions and 35% deletions. No molecule regrowth moves were attempted. Attempts to insert and delete molecules of each species were made with equal probability. Configurational bias sampling techniques were used to increase the number of successful particle insertions [4–6]. Non-coulombic long-range interactions were calculated with the method of Theodorou and Suter [45]. The Ewald summation technique was used for the calculation of electrostatic interactions [46, 47]. Vacuum boundary conditions with 276 k-vectors were used for all simulations.

A volume $V = 10000 \text{ \AA}^3$ was used for all simulations except for water/ethane where $V = 7000 \text{ \AA}^3$ and methanol/ CO_2 where $V = 5000 \text{ \AA}^3$. Except near critical points, system-size effects on the phase behavior for the system sizes studied were within the statistical uncertainties of the simulations. Determination of critical points by mixed-field finite-size scaling methods [18] requires that both pure component and mixture data be extrapolated to infinite-system size. Pure component potential parameters were optimized using a fixed system size [26, 28] and for that reason this analysis was not attempted here for the binary mixtures.

A random initial configuration was used for vapor phase simulations, while liquid phase simulations were started from the final configuration of

a previous run. Simulations were equilibrated for 1 million Monte Carlo Steps (MCS). Vapor phase simulations were run for 5 million MCS, while simulations in the liquid phase were run for 10-20 million MCS. Simulation data were stored in the form of a list containing the number of particles of each species N_1, N_2 and the energy of the system E with samples being taken every 250 MCS. Three independent sets of simulations with different random number seeds were performed for each mixture. The standard deviation of the results of the three simulations sets was used as the statistical uncertainty estimate.

The general strategy of the simulations was to construct the free energy surface over the range of conditions of interest so that phase coexistence properties could be calculated. For this, a link must exist between the liquid and vapor phases. The link was obtained by performing a simulation near the critical point, where the simulation readily fluctuates between liquid and vapor phases. The rest of the phase diagram could then be determined by separate simulations along the liquid and vapor branches of the phase diagram.

For binary mixtures in which one component was supercritical, simulations were first performed near the critical point of the subcritical component. The data were then reweighted to lower temperatures to determine where additional simulations were needed. When the density distributions became sufficiently noisy such that coexistence properties could not be calculated reliably, additional simulations were performed near the predicted coexistence

chemical potentials. Once the temperature of interest was reached, the chemical potential of the second component was increased to introduce molecules of the second type into the system. As for the pure fluid phase envelope, phase coexistence predictions for the mixture were made until the probability distributions became unreliable. The predicted chemical potentials at the point where the simulation data became unreliable were shifted to regions just outside the phase envelope and used as inputs to the next simulation, avoiding metastability problems encountered when the coexistence chemical potentials are used at subcritical conditions. For mixtures where both components were subcritical at the temperature of interest, it was sometimes faster to calculate the pure component phase diagrams of each species and work from each pure component until the two sides met somewhere in the middle of the pressure composition diagram. This was especially useful in systems that display an azeotrope, such as $\text{CH}_3\text{OH}/n$ -hexane.

5 Results and Discussion

5.1 Non-polar/Non-polar and Non-polar/Quadrupolar Mixtures

Some previous results for the phase behavior of mixtures of n -alkanes are available [26] using the same potentials as for the present work. Binary systems studied previously [26] are ethane / n -heptane, ethane / n -decane,

ethane / *n*-eicosane and *n*-octane / *n*-dodecane, using the Lorentz-Berthelot rules for determining unlike-pair interactions. Good agreement with experimental data was obtained for all mixtures studied in [26]. In the present study, both Lorentz-Berthelot and Kong combining rules were used for simulations of *n*-pentane / methane.

Phase diagrams for the isotherms $T = 410.93$ K and 344.26 K are shown in Figure 3. With the histogram-reweighting method, it is possible to calculate phase coexistence properties on an arbitrarily fine grid of temperatures and pressures. For the sake of clarity, however, only two calculated isotherms are presented. The lines shown in the figure are not curve fits to simulation data, but the actual raw simulation data. The average statistical uncertainty in the coexistence pressure is ± 1.0 bar ($1 \text{ bar} = 10^5 \text{ Pa}$), while the average uncertainty in the liquid and vapor mole fractions is ± 0.006 . Potential parameters for unlike-molecule interactions are listed in Table 3. The values predicted by the Lorentz-Berthelot and Kong combining rules are quite similar in this case, with maximum differences of 4 % for the $\text{CH}_2\text{-CH}_4$ well depth. This is due to the fact that the groups which make up the *n*-alkane series have similar size and well depths, and implies that the phase diagrams predicted by each combining rule should also be similar.

It has been demonstrated that for conditions far from the critical point, the effect of system size on the predicted phase envelope is negligible [48]. As the critical point is approached, however, the correlation length becomes larger and diverges at the critical point. Finite-size effects become impor-

tant and the predicted phase behavior becomes a function of system size. Although in principle it is possible to simulate very large systems in order to determine coexistence points in the near critical region, no attempt was made in the present study to do so, due to the heavy computational cost of such calculations. In Figures 3, 6 and 9, only the part of the phase diagram away from the critical point is given for the simulation results, covering the range over which finite-size effects are small.

Agreement of simulation results for both the Lorentz-Berthelot and Kong combining rules with experimental data [49] is good over the entire pressure-composition range studied for the *n*-pentane / methane mixture. This is in contrast to recent Gibbs ensemble simulations of the NERD model [25] for *n*-pentane/methane, which are in good agreement with experiment at low pressure, but have significant deviations at high pressures [32]. The main difference between the NERD model and the model used in the present work is the quality of representation of the pure component vapor pressure curves, which is clearly important for successful predictions of mixture behavior.

N-Alkane/CO₂ mixtures are systems for with molecules made of groups with widely varying potential parameters, as shown in Table 1. For these systems, Kong combining rules give lower values for the unlike-pair interactions potential well depths and higher values for the collision diameters than Lorentz-Berthelot combining rules, as shown in Table 3. In Figure 4, results of simulations for the ethane/CO₂ mixture at $T = 293.15$ K and 263.15 K are shown. The average statistical uncertainty in the coexistence pressure and

mole fractions is ± 0.5 bar and ± 0.005 , respectively. When Lorentz-Berthelot combining rules are used, simulation results differ substantially from experimental values. Simulations predict an azeotrope at much lower pressures than experiment, so the predicted unlike-pair interactions from Lorentz-Berthelot combining rules are too strong in this case. Simulation results for the Kong combining rules, by contrast, are in close agreement with experiment.

Additional simulations were performed for the systems propane/ CO_2 and *n*-pentane/ CO_2 . In Figure 5 we present the pressure-composition diagram for propane/ CO_2 at $T = 327.59$ K and 294.26 K. The pressure-composition diagram for *n*-pentane/ CO_2 at $T = 363.15$ K and 310.15 K is shown in Figure 6. As in the case of ethane/ CO_2 , when Lorentz-Berthelot combining rules are used for the unlike-molecule interactions, the predicted coexistence pressure for a given liquid and vapor composition is too low for both systems. In the case of propane/ CO_2 , the deviation from experiment is greater than for the ethane/ CO_2 system. The deviation from experiment for *n*-pentane/ CO_2 is larger than for propane/ CO_2 . As with ethane/ CO_2 mixture, simulations that used Kong combining rules for unlike-pair interactions yielded results for propane/ CO_2 and *n*-pentane/ CO_2 , shown in Figures 5 and 6, respectively, that were in good agreement with experimental values.

The results of our simulations for *n*-alkane/ CO_2 mixtures suggest that for asymmetric binary mixtures for which neither molecule possesses a strong dipole moment the Lorentz-Berthelot combining rules consistently overpredict unlike-pair interactions, resulting in phase diagrams that deviate signif-

icantly from experiment. Kong combining rules, which give weaker unlike-pair interactions, result in phase diagrams that are in quantitative agreement with experiment. This is an important result as CO₂ is commonly used as a supercritical solvent for polymers [50].

Some additional simulations were performed to investigate the effect of adding partial charges to the ethane model on the ethane/CO₂ mixture phase behavior. Partial charges were added to the original exponential-6 united atom model for ethane at approximately the location of the hydrogen nuclei. The C-H bond length was fixed at 1.090 Å and a fixed C-C-H bond angle of 110.7° was used. The hydrogens were given a partial charge $q_H = +0.06$. To maintain electro-neutrality the charge on each carbon atom was set to $q_C = -0.18$ [39]. The hydrogens on each end of the molecule were staggered 60° from the hydrogens on the opposite end. As previously observed [55], the addition of partial charges had only a small effect on the predicted pure alkane phase behavior, slightly depressing the vapor pressure and increasing the critical temperature. For the ethane/CO₂ mixture, the phase coexistence curve predicted with the charged ethane model (not shown) was within the statistical uncertainties of the coexistence curve predicted by simulations of the non-charged ethane model.

5.2 Polar/Non-polar and Polar/Quadrupolar

Mixtures

Water/ethane is an example of a polar/non-polar mixture. The pressure composition diagram for this system at $T = 573.15$ K is shown in Figure 7. Results for the same mixture and intermolecular potential model with the Lorentz-Berthelot combining rules have been previously obtained from Gibbs-ensemble simulations [33] and are in good agreement with present calculations. Simulation results for the two combining rules are similar, which is not surprising given that the unlike-pair interactions are of similar magnitude (Table 3). While simulation results give a reasonably accurate picture of the phase diagram, they do not agree quantitatively with experimental values above 250 bar. The simulations underpredict the solubility of water in the ethane-rich vapor phase. Earlier results at other temperatures [33] give even larger differences between experimental and predicted equilibrium compositions, with simulations generally underpredicting the solubility of hydrocarbon in the aqueous phase by as much as a factor of two. These differences are possibly due to the lack of polarizability interactions in the water and ethane models, or the use of a completely rigid (inflexible) model for water.

CH₃OH/*n*-hexane is another example of a highly non-ideal polar/non-polar system. In Figure 8 the pressure composition diagram predicted from simulation for $T = 448.15$ K and 398.15 K is shown. Experimental data of Za-

wisza [57] are included for comparison. GCMC histogram-reweighting simulations with Lorentz-Berthelot combining rules correctly predict an azeotrope for both isotherms that lies close to the experimentally determined azeotropic composition and pressure. There are deviations in the simulation data from experiment on the pure methanol side, at least partly due to the fact that the model used in this study for pure methanol underpredicts the vapor pressure by approximately 5% over the entire temperature range. Simulations employing Kong combining rules produced phase coexistence data that was similar to the Lorentz-Berthelot data near the pure *n*-hexane side of the phase diagram. As the mole fraction of methanol in the system is increased, the deviation of the Kong combining rules from the predictions of Lorentz-Berthelot and experimental data also increases. The greatest deviations are seen near the azeotropic point, where the Kong combining rules overpredict the vapor pressure by approximately 6%.

The final system studied was CH₃OH/CO₂. The phase diagram for $T = 313.15$ K is shown in Figure 9. As in the polar/non-polar system CH₃OH/*n*-hexane, Lorentz-Berthelot combining rules yield data in closer agreement with experiment than the Kong combining rules. Considering the large asymmetry in the potential parameters for the groups that make up the methanol and CO₂ models, and the previous success of the Kong combining rules for the *n*-alkane/CO₂ systems, this result suggests that reliable predictions of phase behavior of polar/polar systems may need to incorporate additional interactions (such as polarizability) to allow for reliable predic-

tions of mixture phase behavior from intermolecular potentials optimized to pure component properties. Our reasoning for this conclusion is as follows. For the CH₃OH/*n*-hexane and CH₃OH/CO₂ systems, simulations that use Lorentz-Berthelot combining rules for the unlike-pair interactions are in better agreement with experimental data than those which use the Kong combining rules. The Lorentz-Berthelot combining rules overestimate the dispersive contribution to unlike pair interactions, which compensates for the polarizability interactions between polar and non-polar molecules that is missing from our models. This effect is, presumably, less strong for the non-polar/quadrupolar mixtures such as *n*-alkane/CO₂. These predictions remain to be tested, however, and should be considered tentative at this stage.

6 Conclusions

In this work, potential models developed for pure fluid phase equilibria calculations were tested for their ability to predict mixture phase behavior without introduction of additional empirical parameters. Grand canonical histogram-reweighting Monte Carlo simulations were used to determine mixture phase diagrams to a high accuracy. Two combining rules for obtaining unlike-pair interactions were used, the conventional Lorentz-Berthelot rules and a set of combining rules due to Kong [36] that generally result in less attractive overall unlike-component interactions.

For *n*-alkane/*n*-alkane mixtures, good agreement was found between simulations and experiments using either set of combining rules. For mixtures of components with similar groups, there is little difference in the unlike-pair interactions and thus the predicted phase behavior. For *n*-alkane/CO₂ systems, for which there are significant differences in the predicted phase behavior, the Kong combining rules were found to be significantly better than the Lorentz-Berthelot rules, giving near-quantitative agreement with experiments. This result holds over a homologous series of *n*-alkanes at several temperatures and suggests that there is indeed a good chance of development of quantitative prediction methods for mixture properties from molecular models, without any input from experimental information beyond the pure-component phase behavior. This is a hypothesis that will need to be tested in significantly greater detail than was possible in the present study. Addition of partial charges was found to have no effect on the mixture phase behavior of ethane/CO₂.

In contrast to the behavior seen for the *n*-alkane/CO₂ systems, for polar/non-polar mixtures such as water/ethane and CH₃OH/*n*-hexane and polar/polar mixtures such as CH₃OH/CO₂, the simulation results are often in only qualitative agreement with experimental values and the Lorentz-Berthelot rules are superior to the Kong rules. This observation may be due to deficiencies in the pure component potentials for polar systems, for example the neglect of polarization interactions. Lorentz-Berthelot combining rules result in more attractive unlike-pair interactions, thus possibly compensating

for the lack of polarizability in the models used in this study. It is possible that addition of such interactions to the pure component model will improve significantly the agreement between simulations and experiments for mixtures with a single “universal” combining rule for the dispersive unlike-pair interactions. Testing this hypothesis will be the subject of future work.

7 Acknowledgments

Research on which this manuscript is based was supported the US Department of Energy, Office of Basic Energy Sciences, under grant DEFG02-98ER14014. We would like to thank J. C. Rainwater for bringing reference [52] to our attention.

References

- [1] Panagiotopoulos, A. Z., 1987, *Mol. Phys.*, **61**, 813.
- [2] Panagiotopoulos, A. Z., Quirke, N., Stapleton, M. and Tildesley, D. J., 1988, *Mol. Phys.*, **63**, 527.
- [3] Smit, B. de Smedt, Ph., and Frenkel, D., 1989, *Mol. Phys.* **68**, 931.
- [4] Siepmann, J. I., and Frenkel, D., 1992, *Mol. Phys.*, **75**, 59.
- [5] Frenkel, D., Mooij, G. C. A. M., and Smit, B., 1992, *J. Phys. Cond. Matter*, **4**, 3053.
- [6] De Pablo, J. J., Laso, M., and Suter, U. W., 1992, *J. Chem. Phys.*, **96**, 2395.
- [7] Torrie, G. M., and Valleau, J. P., 1977, *J. Comp. Phys.*, **23**, 187.
- [8] Torrie, G. M., and Valleau, J. P., 1977, *J. Chem. Phys.*, **66**, 1402.
- [9] Valleau, J. P., 1991, *J. Comp. Phys.*, **96**, 193.
- [10] Valleau, J. P., 1993, *J. Chem. Phys.*, **99**, 4718.
- [11] Valleau, J. P., 1999, *Adv. Chem. Phys.*, **105**, 369, edited by D. M. Ferguson, J. I. Siepmann, and D. G. Truhlar (New York: John Wiley and Sons, INC.).
- [12] Kiyohara, K., Spryouni, T., Gubbins, K. E., and Pangiotopoulos, A. Z., 1996, *Mol. Phys.* **89**, 965.

- [13] Escobedo, F. A., and de Pablo, J. J., 1996, *J. Chem. Phys.*, **105**, 4391.
- [14] Ferrenberg, A. M., and Swendsen, R. H., 1988, *Phys. Rev. Lett.*, **61**, 2635.
- [15] Ferrenberg, A. M., and Swendsen, R. H., 1989 *Phys. Rev. Lett.* **63**, 1195.
- [16] Swendsen, R. H., 1993, *Physica A*, **194**, 53.
- [17] Errington, J. R., and Panagiotopoulos, A. Z., 1998, *J. Chem. Phys.*, **109**, 1093.
- [18] Potoff, J. J., and Panagiotopoulos, A. Z., 1998, *J. Chem. Phys.*, **109**, 10914.
- [19] Mon, K. K., and Binder, K., 1992, *J. Chem. Phys.*, **96**, 6989.
- [20] Recht, J. R., and Panagiotopoulos, A. Z., 1993, *Mol. Phys.*, **80**, 843.
- [21] Panagiotopoulos, A. Z., 1994, *Int. J. Thermophys.*, **15**, 1057.
- [22] Valleau, J. P., 1998, *J. Chem. Phys.*, **108**, 2962.
- [23] Wilding, N. B., 1995, *Phys. Rev. E*, **52**, 602.
- [24] Martin, M. G., and Siepmann, J. I., 1998, *J. Phys. Chem. B*, **102**, 2569.
- [25] Nath, S. K., Escobedo, F. A., and de Pablo, J. J., 1998, *J. Chem. Phys.*, **108**, 9905.

- [26] Errington, J. R., and Panagiotopoulos, A. Z., *J. Phys. Chem. B* (submitted).
- [27] Harris, J. G., and Yung, K.H., 1995, *J. Phys. Chem.*, **99**, 12021.
- [28] Errington, J. R., and Panagiotopoulos, A. Z., 1999, manuscript in preparation.
- [29] Errington, J. R., and Panagiotopoulos, A. Z., 1998, *J. Phys. Chem. B*, **102**, 7470.
- [30] Martin, M. G., and Siepmann, J. I., 1997, *J. Am. Chem. Soc.*, 1997, **119**, 8921.
- [31] Spyriouni, T., Economou, I. G., and Theodorou, D. N., 1998, *Phys. Rev. Lett.*, **80**, 4466.
- [32] Nath, S. K., Escobedo, F. A., de Pablo, J. J., and Patramai, I., 1998, *Ind. Eng. Chem. Res.*, **37**, 3195.
- [33] Errington, J. R., Boulougouris, G. C., Economou, I. G., Panagiotopoulos, A. Z., and, Theodorou, D. N., 1998, *J. Phys. Chem. B*, **102**, 8865.
- [34] Mackie, A. D., Tavitian, B., Boutin, A., and Fuchs, A. H., 1997, *Molec. Simulation* **19**, 1.
- [35] Maitland, G. C., Rigby, M., Smith, E. B., and Wakeham, W. A., 1981, *Intermolecular Forces* (Oxford: Clarendon Press), pp. 519-523.

- [36] Kong, C. L., 1973, *J. Chem. Phys.*, **59**, 2464.
- [37] Berg, B. A., and Neuhaus, T., 1992, *Phys. Rev. Lett.*, **68**, 9.
- [38] Van der Ploeg, P., and Berendsen, H. J. C., 1982, *J. Chem. Phys.*, **84**, 3271.
- [39] Jorgensen, W. L., Maxwell, D. S., and Tirado-Rives, J., 1996, *J. Am. Chem. Soc.*, **118** 11225.
- [40] Jorgensen, W. L., Madura, J. D., and Swenson, C. J., 1984, *J. Am. Chem. Soc.*, **106**, 813.
- [41] Smit, B., Karaborni, S., and Siepmann, J. I., 1995, *J. Chem. Phys.*, **102**, 2126.
- [42] Dodd, L. R. and Sandler S. I., 1991, *Fluid Phase Equil.*, **63**, 279.
- [43] Fender, B. E. F., and Halsey Jr., G. D., 1962, *J. Chem. Phys.*, **36**, 1881.
- [44] Smith, F. T., 1972, *Phys. Rev. A*, **5**, 1708.
- [45] Theodorou, D. N., and Suter, U. W., 1985, *J. Chem. Phys.*, **82**, 955.
- [46] de Leeuw, S. W., Perram, J. W., and Smith, E. R., 1980, *Proc. R. Soc. Lond. A*, **373**, 27.
- [47] Smith, A. P., and Ashcroft, N. W., 1988, *Phys. Rev. B.*, **38**, 12942.

- [48] Orkoulas, G., and Panagiotopolous, A. Z., 1999, *J. Chem. Phys.*, **110**, 1581.
- [49] Berry, V. M., and Sage, B. H., 1970, *NSRDS-NBS*, **32**.
- [50] Catchpole, O. J., Grey, J. B., and Noermark, K. A., 1998, *J. Chem. Eng. Data*, **43**, 1091.
- [51] Fredenslund, A., and Mollerup, J., 1974, *J. Chem. Soc. Faraday Transactions I*, **70**, 1653.
- [52] Niesen, V. G., and Rainwater, J. C., 1990, *J. Chem. Thermodynamics*, **22**, 777.
- [53] Reamer, H. H., Sage, B. H., and Lacey, W. N., *Ind. Eng. Chem.*, **43**, 2515.
- [54] Tochigi, K., Hasegawa, K., Asano, N., and Kojima, K., 1998, *J. Chem. Eng. Data*, **43**, 954.
- [55] Chen, B., Martin, M. G., and Siepmann, J. I., 1998, *J. Phys. Chem. B*, **102**, 2578.
- [56] Danneil, A., Toedheide, K., and Frank, E. U., 1967, *Chemie-Ing. Techn.*, **39**, 816.
- [57] Zawisza, A., 1985, *J. Chem. Thermodynamics*, **17**, 941.
- [58] Ohgaki, K., and Katayama, T., 1976, *J. Chem. Eng. Data*, **21**, 53.

Table 1: Potential parameters

Group	$\varepsilon/k_b/K$	$\sigma/\text{\AA}$	α	Charge
CH ₃ (in <i>n</i> -alkanes)	129.64	3.679	16.0	0.0
CH ₂ (in <i>n</i> -alkanes)	73.50	4.000	22.0	0.0
C (in CO ₂)	29.07	2.753	14.0	+0.6466
O (in CO ₂)	83.20	3.029	14.0	-0.3233
O (in H ₂ O)	159.78	3.1947	12.0	-0.7374
H (in H ₂ O)	-	-	-	+0.3687
CH ₃ (in CH ₃ OH)	129.64	3.679	16.0	+0.2704
O (in CH ₃ OH)	97.00	3.100	16.0	-0.7140
H (in OH of CH ₃ OH)	-	-	-	+0.4436

Table 2: Group Distances

Group-Group	Distance / Å
CH ₃ -CH ₃	1.839
CH ₃ -CH ₂	1.687
CH ₂ -CH ₂	1.535
C-O (in CO ₂)	1.1433
O-H (in H ₂ O)	1.0668
CH ₃ -O (in CH ₃ OH)	1.425
O-H (in CH ₃ OH)	0.945

Table 3: Unlike-Pair Interactions

Group	Mixture	$1 - \frac{\epsilon_{Kong}}{\epsilon_{L-B}}$	$1 - \frac{\sigma_{Kong}}{\sigma_{L-B}}$	$1 - \frac{\alpha_{Kong}}{\alpha_{L-B}}$
CH ₃ -CH ₄	<i>n</i> -pentane/methane	0.004	-0.0007	0.0002
CH ₂ -CH ₄	<i>n</i> -pentane/methane	0.038	-0.0082	0.0063
C-CH ₃	<i>n</i> -alkane/CO ₂	0.115	-0.0145	-0.0206
C-CH ₂	<i>n</i> -alkane/CO ₂	0.101	-0.0088	-0.0218
O-CH ₃	<i>n</i> -alkane/CO ₂	0.040	-0.0042	-0.0079
O-CH ₂	<i>n</i> -alkane/CO ₂	0.065	-0.0081	-0.0103
CH ₂ -CH ₃	<i>n</i> -hexane/CH ₃ OH	0.023	-0.0046	0.0031
CH ₃ -O	<i>n</i> -hexane/CH ₃ OH	0.040	-0.0037	-0.0034
CH ₂ -O	<i>n</i> -hexane/CH ₃ OH	0.056	-0.0053	-0.0112
O-CH ₃	water/ethane	0.024	-0.0058	-0.0031
C-CH ₃	CO ₂ /CH ₃ OH	0.115	-0.0145	-0.0206
O-CH ₃	CO ₂ /CH ₃ OH	0.040	-0.0042	-0.0079
C-O	CO ₂ /CH ₃ OH	0.008	0.0446	-0.0018
O-O	CO ₂ /CH ₃ OH	-0.002	0.0002	0.0020

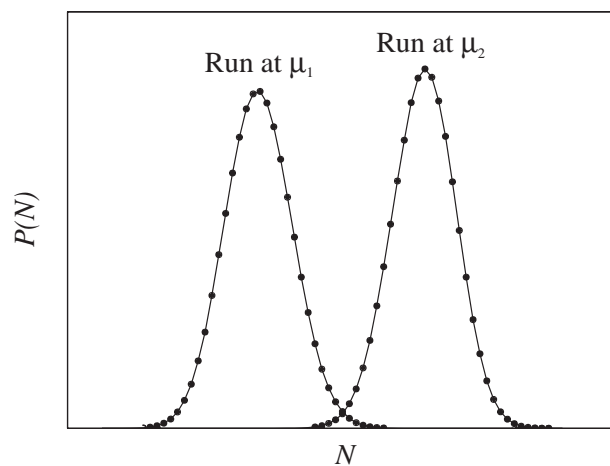


Figure 1: Schematic diagram of histogram collection for two grand canonical Monte Carlo simulations at different chemical potentials.

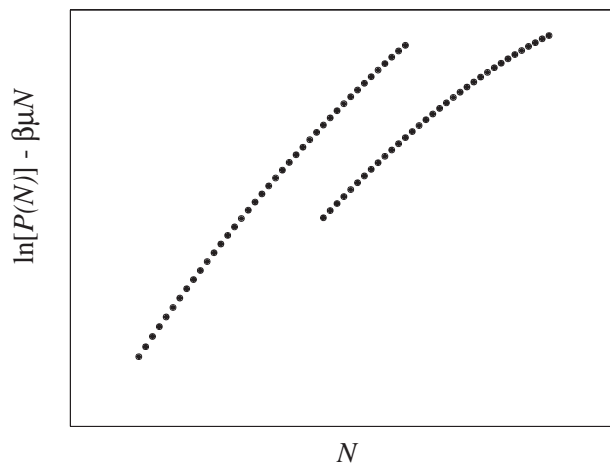


Figure 2: Schematic diagram of histogram transformation for determination of the free energy over a broad range of densities.

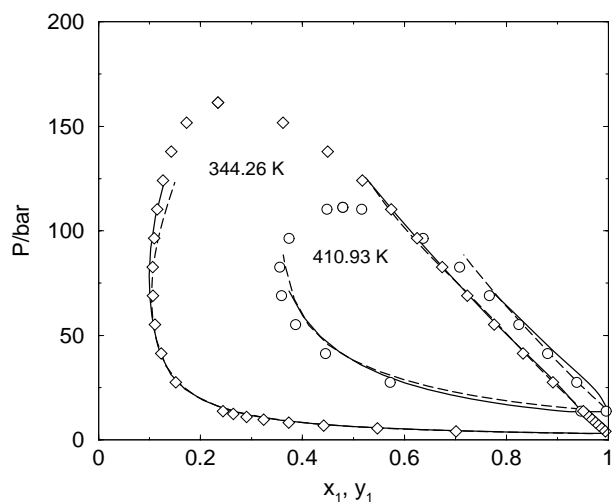


Figure 3: *n*-Pentane/methane pressure composition diagram. Experimental data: $T = 410.93$ K (open circles), $T = 344.26$ K (open diamonds) [49]. $1 \text{ bar} = 10^5 \text{ Pa}$. GCMC simulations with the Lorentz-Berthelot (solid line) and Kong combining rules (dashed line). The average statistical uncertainties for the simulation data in pressure and composition are ± 0.98 bar and ± 0.0055 , respectively.

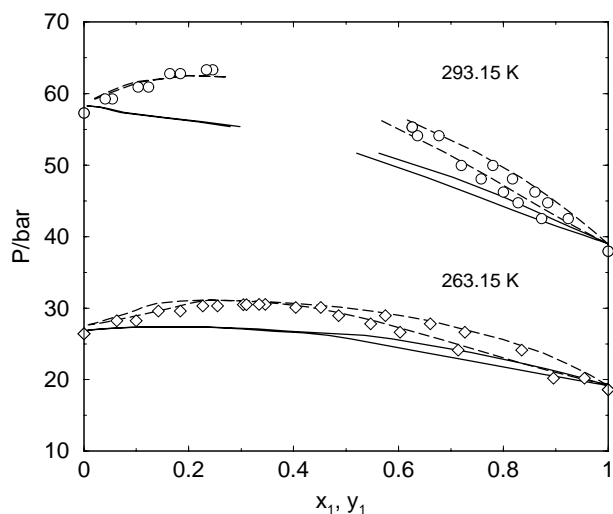


Figure 4: Ethane/CO₂ pressure composition diagram. Experimental data: $T = 293.15$ K (open circles), $T = 263.15$ K (open diamonds) [51]. 1 bar = 10^5 Pa. GCMC simulations with the Lorentz-Berthelot (solid line) and Kong combining rules (dashed line). The average statistical uncertainties for the simulation data in pressure and composition are ± 0.51 bar and ± 0.0045 , respectively.

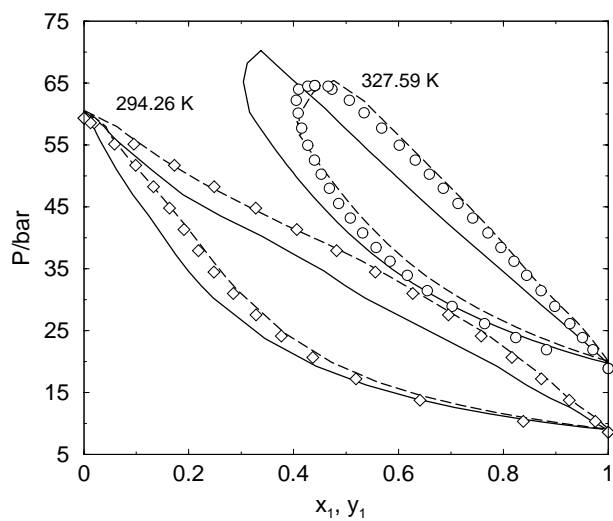


Figure 5: Propane/CO₂ pressure composition diagram. Experimental data: $T = 327.59$ K (open circles) [52], $T = 294.26$ K (open diamonds) [53]. 1 bar = 10^5 Pa. GCMC simulations with the Lorentz-Berthelot (solid line) and Kong combining rules (dashed line). The average statistical uncertainties for the simulation data in pressure and composition are ± 0.47 bar and ± 0.0050 , respectively.

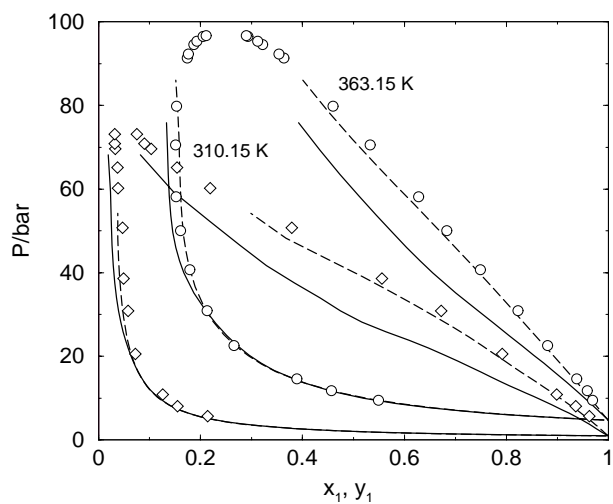


Figure 6: *n*-Pentane/CO₂ pressure composition diagram. Experimental data: $T = 363.15$ K (open circles), $T = 310.15$ K (open diamonds) [54]. 1 bar = 10^5 Pa. GCMC simulations with the Lorentz-Berthelot (solid line) and Kong combining rules (dashed line). The average statistical uncertainties for the simulation data in pressure and composition are ± 0.30 bar and ± 0.0027 , respectively.

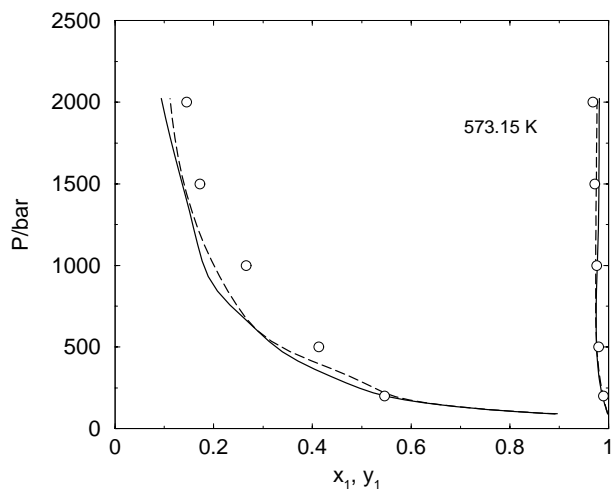


Figure 7: $\text{H}_2\text{O}/\text{ethane}$ pressure composition diagram at $T = 573.15 \text{ K}$. Experimental data (open circles), [56]. $1 \text{ bar} = 10^5 \text{ Pa}$. GCMC simulations with the Lorentz-Berthelot (solid line) and Kong combining rules (dashed line). The average statistical uncertainties for the simulation data in pressure, liquid phase and vapor phase composition are $\pm 0.90 \text{ bar}$, ± 0.003 and ± 0.010 respectively.

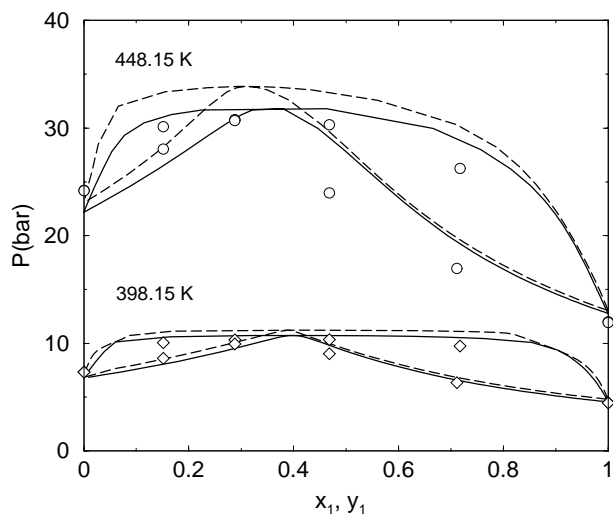


Figure 8: $\text{CH}_3\text{OH}/n\text{-hexane}$ pressure composition diagram. Experimental data: $T = 448.15$ K (open circles), $T = 398.15$ K (open diamonds) [57]. $1 \text{ bar} = 10^5 \text{ Pa}$. GCMC simulations with the Lorentz-Berthelot (solid line) and Kong combining rules (dashed line). The average statistical uncertainties for the simulation data in pressure and composition are ± 0.43 bar and ± 0.015 , respectively.

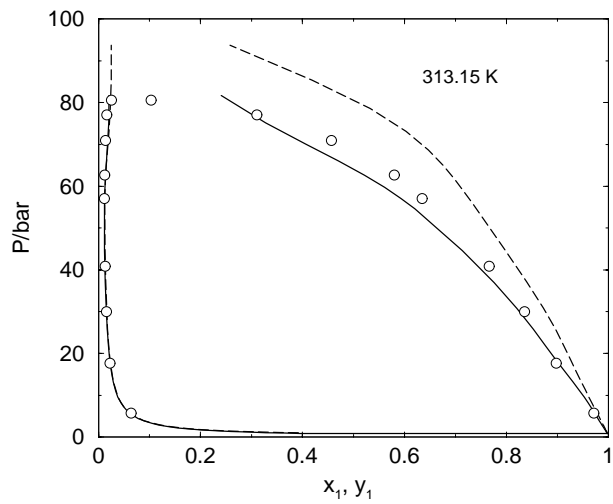


Figure 9: $\text{CH}_3\text{OH}/\text{CO}_2$ pressure composition diagram at $T = 313.15 \text{ K}$. $1 \text{ bar} = 10^5 \text{ Pa}$. Experimental data (open circles), [58]. GCMC simulations with the Lorentz-Berthelot (solid line) and Kong combining rules (dashed line).